

# Electrospun Electroluminescent CsPbBr<sub>3</sub> Fibers as Flexible Perovskite Networks for Light-Emitting Application

Khan Lê, Florian von Toperczer, Feray Ünlü, Gopinath Paramasivam, Florian Mathies, Edgar Nandayapa, Emil J. W. List-Kratochvil, Thomas Fischer, Klas Lindfors, and Sanjay Mathur\*

Thin-film perovskite light-emitting diodes have gained increasing attention in the last 6 years. With the possibility to process the emitting layer from solution, the way for 1D morphology of the semiconductor for flexible devices is paved. Herein, for the first time single-step fabrication of CsPbBr<sub>3</sub>@PVP nanofibers in a customized electrospinning process performed under ambient conditions from a water-based precursor solution is reported. The water-based approach allows the incorporation of a conductive polymer into the compound fiber by blending the perovskite precursor ink with commercially available PEDOT:PSS dispersion. The results demonstrate electrospun fiber mats which are stable at ambient conditions for at least 5 months and can be utilized in electroluminescence devices. Photoluminescence studies on the perovskite fibers reveal a blueshift of the emission peak compared to thin films possibly due to the generation of nanocrystals of  $\approx 12$  nm by in situ nanocrystal pinning as confirmed by transmission electron microscopy. A proof-of-concept electrically pumped light-emitting device is built with the obtained fiber mat. The perovskite nanofibers offer promising applications in flexible and stretchable optoelectronics.

integration in the device.<sup>[3–5]</sup> The nanocrystals show exceptionally high photoluminescence quantum yield (PLQY) of almost unity.<sup>[6]</sup> However, alternative morphologies like fiber-shaped active materials are less explored. There are examples of CsPbI<sub>3</sub> nanowire clusters with enhanced stability compared to their thin-film counterpart.<sup>[7]</sup> First steps toward optoelectronic fibrous lead halide perovskite devices were made by Fu et al. who electrospun PbI<sub>2</sub> fibers and subsequently treated them with CH<sub>3</sub>NH<sub>3</sub>I in solution to obtain CH<sub>3</sub>NH<sub>3</sub>PbI<sub>3</sub> fibers. They suggested their use in ammonia sensors.<sup>[8]</sup> Furthermore, photodetectors made from electrospun PAN/CH<sub>3</sub>NH<sub>3</sub>PbI<sub>3</sub> fibers were reported by Li et al.<sup>[9]</sup> For photovoltaic applications, Chen and Zhu integrated CH<sub>3</sub>NH<sub>3</sub>PbI<sub>3</sub> fibers in dye-sensitized solar cells.<sup>[10]</sup> The influence of polymer content on the fiber morphology was investigated for CH<sub>3</sub>NH<sub>3</sub>PbI<sub>3</sub>/PVP fibers and in addition,


they were successfully integrated into solid-state solar cells by Bohr et al.<sup>[11]</sup>

Regarding electroluminescent perovskite fibers, there are only reports on macroscopic fibers. For example, carbon nanotube fibers (diameter:  $\approx 23$   $\mu$ m) were coated with blade-applied perovskite active material and silver nanowires as a second electrode by Alivisatos and co-workers.<sup>[12]</sup> Polymeric fibers dip coated with poly(3,4-ethylenedioxythiophen)-polystyrene sulfonate (PEDOT:PSS), perovskite, and silver nanowires were demonstrated by Zeng and

## 1. Introduction

Organic–inorganic lead halide perovskites were recently explored as the emitting layer for room-temperature electroluminescence (EL) devices.<sup>[1]</sup> All-inorganic lead halide perovskites offer better stability than their organic hybrid counterparts.<sup>[2]</sup> The current perovskite light-emitting-diode (PeLED) material research focuses either on the preparation of CsPbX<sub>3</sub> as thin films from precursor solutions or as nanocrystals that are synthesized before

K. Lê, T. Fischer, S. Mathur  
Institute of Inorganic Chemistry  
University of Cologne  
Greinstr. 6, 50939 Cologne, Germany  
E-mail: sanjay.mathur@uni-koeln.de

 The ORCID identification number(s) for the author(s) of this article can be found under <https://doi.org/10.1002/adem.202201651>.

© 2023 The Authors. Advanced Engineering Materials published by Wiley-VCH GmbH. This is an open access article under the terms of the Creative Commons Attribution-NonCommercial License, which permits use, distribution and reproduction in any medium, provided the original work is properly cited and is not used for commercial purposes.

DOI: 10.1002/adem.202201651

F. von Toperczer, K. Lindfors  
Institute of Physical Chemistry  
University of Cologne  
Greinstr. 4-6, 50939 Cologne, Germany

F. Ünlü, G. Paramasivam, F. Mathies, E. Nandayapa,  
E. J. W. List-Kratochvil  
Solution Processing of Hybrid Materials & Devices  
Helmholtz-Zentrum Berlin für Materialien und Energie GmbH  
Hahn-Meitner-Platz 1, 14109 Berlin, Germany

E. J. W. List-Kratochvil  
Institut für Physik  
Institut für Chemie  
IRIS Adlershof  
Humboldt-Universität zu Berlin  
Zum Großen Windkanal 2, 12489 Berlin, Germany

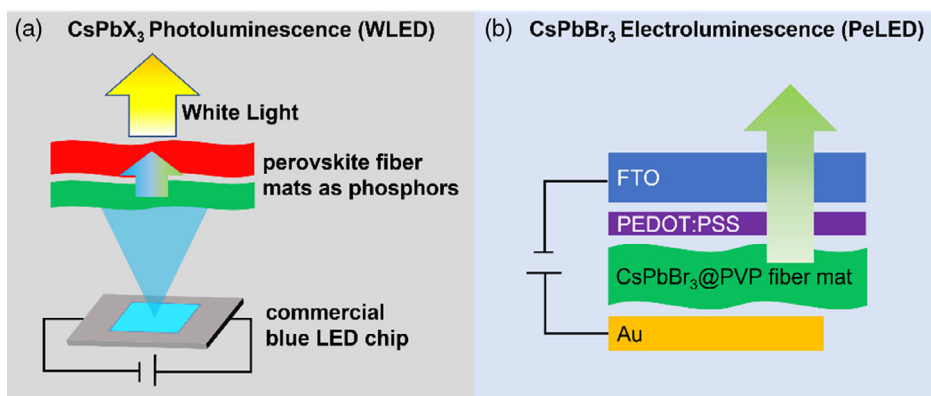


**Figure 1.** Comparison of a) optically pumped WLED devices. Adapted with permission from.<sup>[33]</sup> Copyright 2018, American Chemical Society.<sup>[33]</sup> b) electrically pumped perovskite devices prepared in this work.

co-workers.<sup>[13]</sup> To the best of our knowledge, nanoscale perovskite fibers were only explored for optically pumped white light-emitting diodes (WLEDs) in which they are applied on top of a commercial LED acting as the pump (**Figure 1a**). For the WLEDs, the perovskite is either prepared in nanocrystalline form (“quantum dots”) before spinning with a polymer<sup>[14]</sup> or the perovskite fibers are prepared from a precursor solution directly mixed with the polymer to crystallize during or after the spinning process.<sup>[15]</sup>

The one-step synthesis of CsPbBr<sub>3</sub>@polymer nanofibers by an electrospinning process was reported by Zhang et al. who obtained aligned perovskite nanorods with tailored aspect ratios in polystyrene.<sup>[16]</sup> Chen et al. embedded CsPbBr<sub>3</sub> nanocrystals in polystyrene fibers for nanoscopic imaging<sup>[17]</sup> and Zhang et al. exploited the photocatalytic properties of the perovskite in polymethyl methacrylate matrix for degradation of various organic dyes.<sup>[18]</sup> Especially the use of polystyrene shows good stability as determined by complete PLQY retention after storage under ambient conditions for 18 months<sup>[19]</sup> or 83% PLQY retention after being immersed in water for 3 months.<sup>[14]</sup>

In this work, we present cesium lead bromide (CsPbBr<sub>3</sub>) fibers supported by a polyvinylpyrrolidone (PVP) matrix, synthesized by a one-step electrospinning method from an water- and ionic liquid-based green solvent spinning solution. The insulating polymer remains as supporting matrix and provides flexibility and nanocrystal stabilization. Compounding the spinning solution with PEDOT:PSS yielded fibers with sufficient conductivity for electrically activated luminescence. We investigated the photoluminescence (PL) characteristics and built a proof-of-concept electroluminescent nanofiber device. To the best of our knowledge, this is the first report on electrically pumped nanofiber PeLEDs.

## 2. Results and Discussion

The CsPbBr<sub>3</sub>/PVP nanofibers were prepared by a one-step electrospinning process under ambient conditions from an H<sub>2</sub>O/EtOH solution mixed with the protic ionic liquid methylammonium propionate<sup>[20]</sup> with PVP as the polymer matrix. Utilization of water and ethanol as solvents has two major advantages: first, they are nontoxic solvents and second, they allow mixing of the spinning solution with commercially available, aqueous PEDOT:

PSS dispersion, which provides the conductivity needed for electrical excitation of the fibers. The PVP matrix (alone) is insulating. The CsPbBr<sub>3</sub>/polymer fibers were spun on glass or fluorine-doped tin oxide (FTO) substrates over a hotplate set to 180 °C to aid in solvent evaporation, as fibers spun at ambient temperature tend to dissolve during the electrospinning process, as shown from Figure S1a,b, Supporting Information. Ethanol was utilized to reduce the surface tension of the spinning solution to counteract bead formation occurring for the pure water-based solution (visible in Figure S1c, Supporting Information). The protic ionic liquid (methylammonium propionate, MAP) and formic acid were necessary for full dissolution of CsBr and PbBr<sub>2</sub> in the H<sub>2</sub>O/EtOH mixture at 60 °C and stabilization of the solution at room temperature. The electrospinning parameters are listed in **Table 1**.

The obtained CsPbBr<sub>3</sub>/PVP nanofibers have an average diameter of 120 ± 33 nm, determined by evaluation of scanning electron microscopy (SEM) images (**Figure 2a,b**). Calcination of the fibers was avoided, as the flexibility provided by the polymeric matrix was desired. Thus, the X-ray diffraction (XRD) pattern of the CsPbBr<sub>3</sub>/PVP/PEDOT:PSS composite (**Figure 2c**) was directly measured with the as-spun fibers, so the residing amorphous phase and polymers result in a slightly distorted baseline. Nevertheless, the XRD data confirm the formation of CsPbBr<sub>3</sub> (JCPDS reference 18-0364) with the (110) peak being the most pronounced and the main reflexes indexed as 15.08° (100), 21.32° (110), 26.39° (111), 30.55° (200), 34.19° (210), 37.61° (211), and 43.61° (220). In addition, there is a minor phase of Cs<sub>4</sub>PbBr<sub>6</sub> (JCPDS reference 73-2478) indexed with a star (\*), since excess CsBr (1.2 eq. CsBr/1.0 eq. PbBr<sub>2</sub>) was utilized to increase the luminescence and reduce metallic Pb in the compound as reported elsewhere.<sup>[21,22]</sup> The crystallite size of

**Table 1.** Parameters for electrospinning the CsPbBr<sub>3</sub>/polymer composite nanofibers.

Syringe Volume	Needle	Feed Rate	Voltage	Distance (spinneret to collector)	Substrate Temperature
6 mL	21-gauge, inner Ø 0.514 mm	7 µL min <sup>-1</sup>	17 kV	8 cm	180 °C

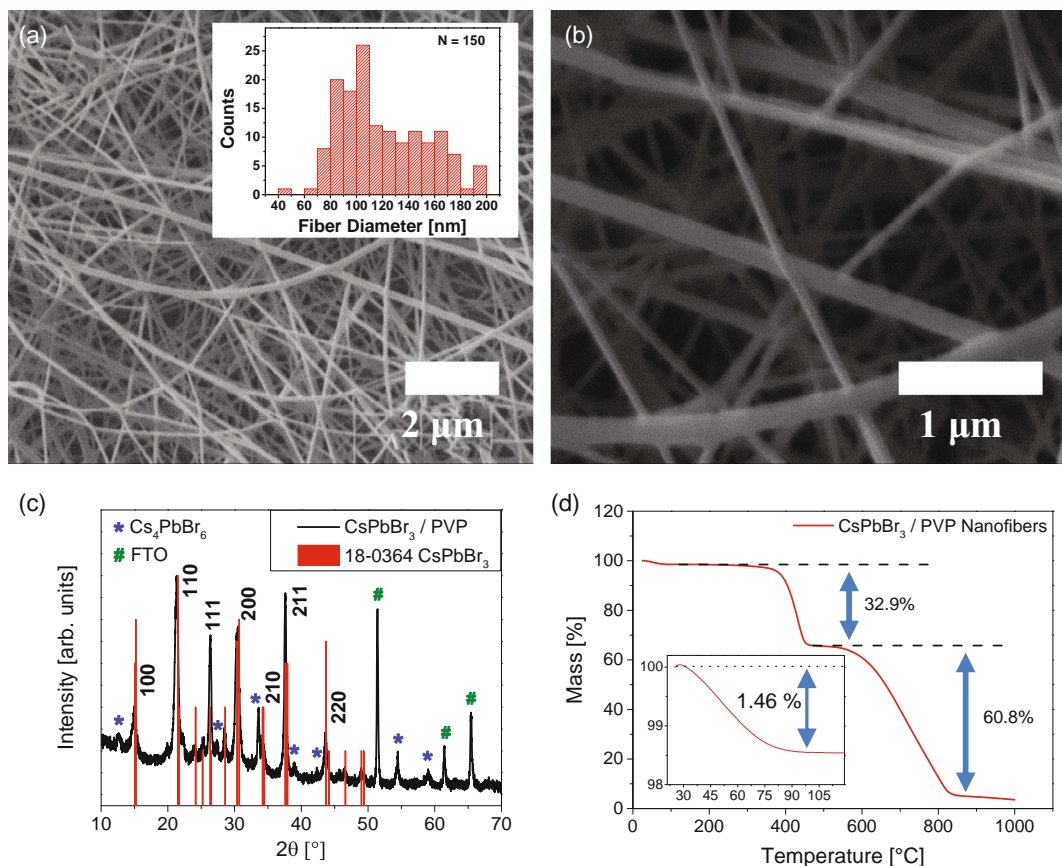


**Figure 2.** SEM micrographs of a) CsPbBr<sub>3</sub> fibers electrospun from H<sub>2</sub>O/EtOH and b) PEDOT:PSS compound CsPbBr<sub>3</sub> nanofibers. The inset shows the histogram of fiber diameter measurements. c) XRD of CsPbBr<sub>3</sub>/PVP fibers on a FTO substrate. The minor Cs<sub>4</sub>PbBr<sub>6</sub> phase is denoted with a star (\*) and the reflexes of the FTO substrate are indexed with a hash (#). d) TG measurement of the PVP fibers in air. The inset shows the first mass loss in detail.

the perovskite was approximated as  $8.4 \pm 2.7$  nm with the Scherrer equation (Equation (1))

$$L = \frac{K \cdot \lambda}{\Delta(2\theta) \cdot \cos \theta_0} \quad (1)$$

with  $K$  being the shape factor ( $K = 0.9$  under the assumption of spherical shape),  $\lambda$  the wavelength of the X-ray ( $M\alpha K\alpha = 0.07107$  nm),  $\theta_0$  the Bragg angle ( $2\theta/2$ ), and  $\Delta(2\theta)$  the full width at half maximum (FWHM) of the reflex, both in radians.

Thermogravimetry (TG) (Figure 2d) was conducted to determine the perovskite/polymer ratio of the obtained fibers. In the first step of decomposition, a mass loss of 1.46% occurred up to  $\approx 100$  °C due to the release of adsorbed or residual water (Figure 2d, inset). Between 350 °C and 450 °C, the PVP decomposes,<sup>[23]</sup> resulting in a mass loss of 32.9%, which is followed by a mass loss of 60.8% between 500 and 900 °C as the CsPbBr<sub>3</sub> perovskite decomposes, as it was shown in the literature.<sup>[2]</sup>

The scanning transmission electron (Figure 3a,b) and transmission electron micrograph (Figure 3c) reveal nanocrystallites with a size of  $12 \pm 3$  nm (Figure 3a, inset) embedded in the polymer matrix. The fast crystallization attributed to the electrospinning parameters combined with confinement in the polymer matrix seems to inhibit the crystal growth, generating nanocrystals in situ. This phenomenon of nanocrystal pinning by the

addition of polymers into perovskite precursor inks has been reported for spin-coated thin films.<sup>[24–27]</sup> The observed rings in the selected-area electron diffraction (SAED) (Figure 3d) confirm the polycrystalline nature of the material with the two dominant lattice planes corresponding to (111) and (210). The energy-dispersive X-ray (EDX) spectroscopy mapping (Figure S2, Supporting Information) shows a homogeneous distribution of Cs, Pb, and Br throughout the fiber. Low count rates for Cs, Pb, and Br in comparison to high counts of Cu (due to the two copper grids used to fix the TEM sample) hindered the determination of elemental ratios.

The UV/vis extinction spectrum shows the absorption edge starting from  $\approx 515$  nm (Figure 4a) and a local maximum at  $\approx 510$  nm. This corresponds to the absorption of similar-sized CsPbBr<sub>3</sub> nanocrystals by Zhang et al.<sup>[28]</sup> The Tauc plot for a direct-bandgap semiconductor was calculated and a bandgap of 2.21 eV was obtained (Figure 4b), being close to reported values of around 2.25 eV.<sup>[29,30]</sup>

The PL micrograph (Figure 5a) confirms the homogenous distribution of luminescent perovskite nanocrystals within the fibers, as it shows evenly distributed emission throughout the fibers with intersecting parts appearing with higher intensity. The PL spectrum (Figure 5b) shows a peak centered at 510 nm which is slightly blueshifted compared to thin films of CsPbBr<sub>3</sub> ( $\approx 525$  nm).<sup>[5]</sup> The FWHM was determined as 19.35 nm from a Gaussian fit function. As the perovskite is pinned as  $\approx 12$  nm crystals within the

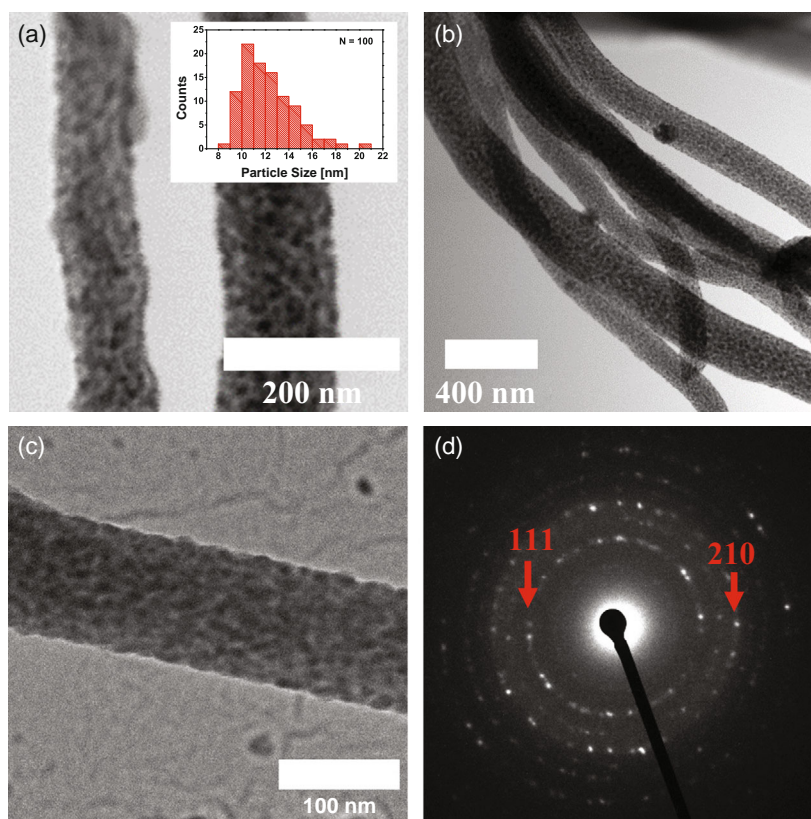


**Figure 3.** a,b) STEM with the inset showing the particle size histogram. c) TEM and d) SAED of the CsPbBr<sub>3</sub>/PVP fibers.

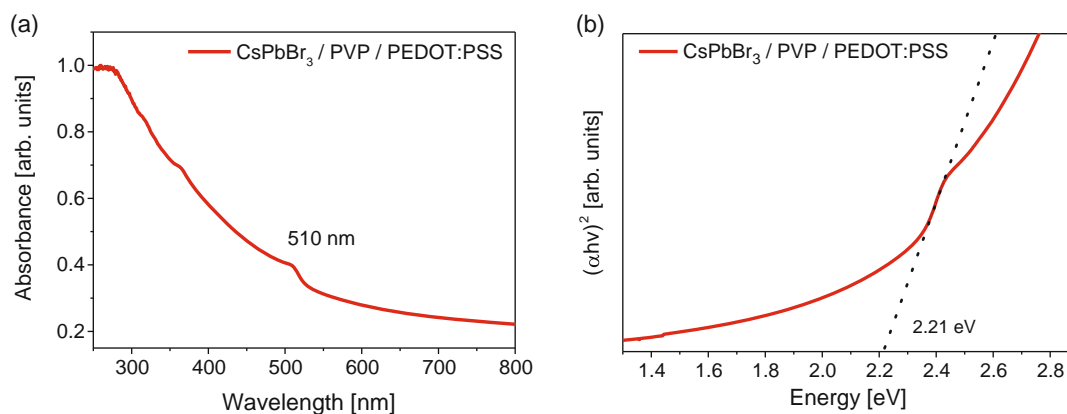


**Figure 4.** a) UV/vis extinction spectrum of the CsPbBr<sub>3</sub>/PVP fibers and b) Tauc plot calculated from the UV/vis extinction spectrum with an extracted bandgap of 2.21 eV.

polymer matrix, this blueshift can arise due to quantum confinement, as discussed for nanocrystals in the literature.<sup>[31,32]</sup> The PLQY of the CsPbBr<sub>3</sub>@PVP fibers was determined as 18.66%.

We further explored the relationship between fiber diameter and optical properties, as up to a certain threshold, the crystallite size confined within the fibers should stay the same (since the crystallite sizes are much smaller than the fiber diameter). Fiber diameters between  $60 \pm 14$  and  $120 \pm 33$  nm were obtained by variation of either the voltage applied (12–25 kV) or variation of the PVP concentration in the spinning solution (46.87,

62.50, 78.13 mg mL<sup>-1</sup>). The utilized parameters and fiber diameters are listed in Table S1, Supporting Information, and the respective SEM micrographs and size histograms are shown in Figure S3, Supporting Information. As expected, the UV/vis extinction spectra (**Figure 6**) show that the local absorption maxima are almost equal within this size regime. It must be noted that the absorption maxima of the fiber diameter variation samples are 6 nm redshifted compared to the sample presented in Figure 4a (with  $\lambda_{\text{peak}} = 510$  nm), which could be due to slightly different processing parameters (humidity, substrate

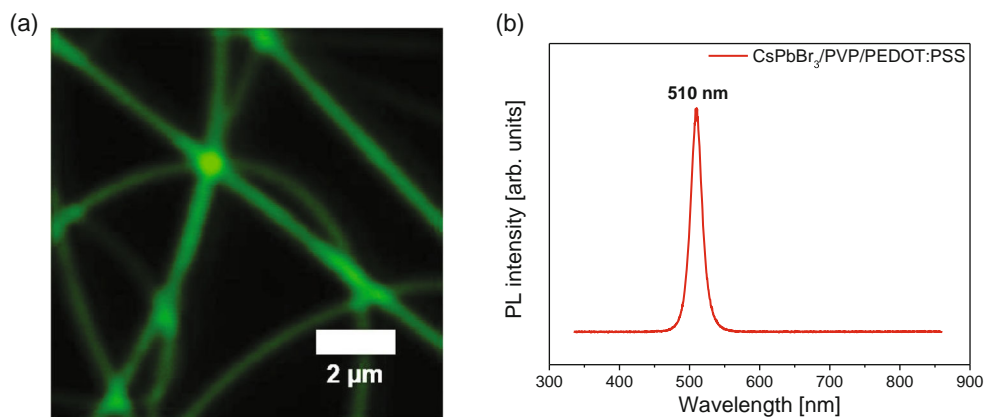


**Figure 5.** a) PL micrograph and b) PL spectrum of the CsPbBr<sub>3</sub>/PVP fibers. The excitation wavelength was 433 nm (see also Experimental Section).

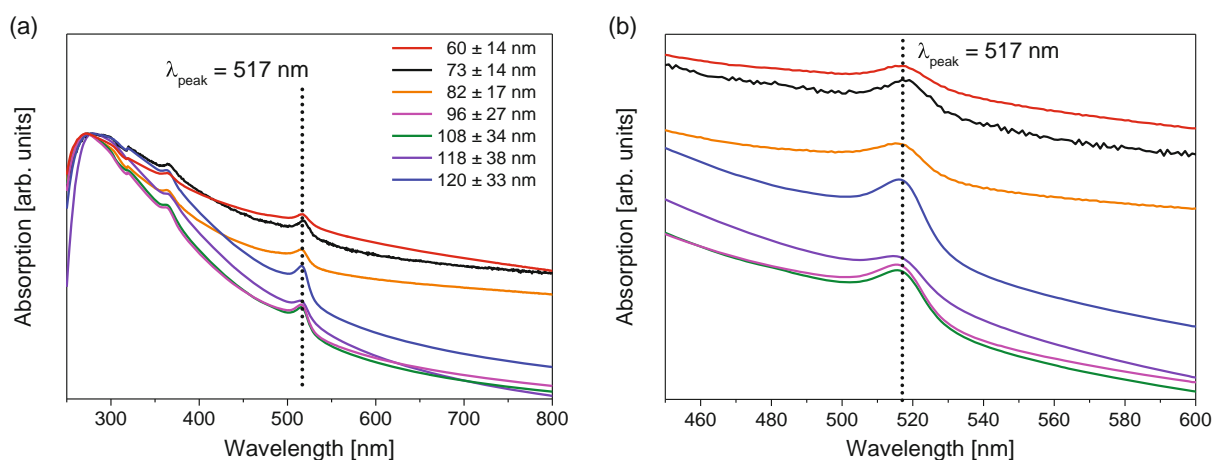


**Figure 6.** a) UV/vis extinction spectra of the CsPbBr<sub>3</sub>/polymer composite fibers with different diameters from 60 to 120 nm as denoted in the graph. b) Detailed view of the region around the 517 nm peak.

temperature, weighing errors) which ultimately could have an impact on the crystallization since the diameter-variation samples were all prepared on the same day but the initial UV/vis and PL sample was prepared on another day. The stability of the H<sub>2</sub>O/MAP/CsPbBr<sub>3</sub> precursor ink was proven over 1 month by <sup>257</sup>Pb and <sup>133</sup>Cs NMR (Figure S4, Supporting Information) and the stability of the fiber mats over 5 months by UV/vis extinction spectra, SEM, and XRD (Figure S5, Supporting Information). The fiber mats were stored in normal laboratory atmosphere (≈20–25 °C; 60%–80% RH; air; no direct sunlight) for 5 months. The CsPbBr<sub>3</sub> fiber stability was further tested by heat treatment at 300 °C for 4 h and illumination under 1 sun (1.5 AM, 100 W) for 4 h. After the heat treatment, the PL of the perovskite fibers is almost completely lost, while the illuminated sample only lost ≈30% of the initial PL intensity. PL spectra after the treatments are shown in SI (Figure S10, Supporting Information).

## 2.1. Proof-of-Concept Device

As a proof of concept, a light-emitting diode was built by electrospinning the perovskite fibers on a PEDOT:PSS-coated FTO

substrate followed by thermal evaporation of 100 nm gold as the back electrode. Photographs of the device under normal light and UV are shown in **Figure 7a,b**. Application of a 5 V bias leads to a visible EL (Figure 7c,d). Indium–gallium–tin eutectic was utilized on top of the gold electrode (Figure 7e) as rigid electrode in direct contact with the gold electrode scratched the fibers and the gold from the substrate and thereby led to short circuit.

From the photographs of the prepared LED (Figure 7c,d) it is visible that the designated active area (the area of the evaporated gold electrode) is not fully luminescent. This is probably attributed to favored charge injection over the interface of the gallium–indium–tin–eutectic and gold. Furthermore, even the spot where the liquid metal electrode is residing is not fully functional. The dark spots could remain as a result of either accumulation of insulating PVP matrix and therefore bad interconnectivity of the CsPbBr<sub>3</sub> nanocrystals (**Figure 8a**) or bad contact of electrodes and perovskite fiber mat on a macroscopic scale as the fiber mat is not flat (Figure 8c). Proof of the intact fiber structure after gold evaporation can be seen from the SEM micrographs in Figure S6, Supporting Information, where areas of the device with and without evaporated gold are shown. Furthermore, Figure S6, Supporting Information reveals that the gold covers the fiber

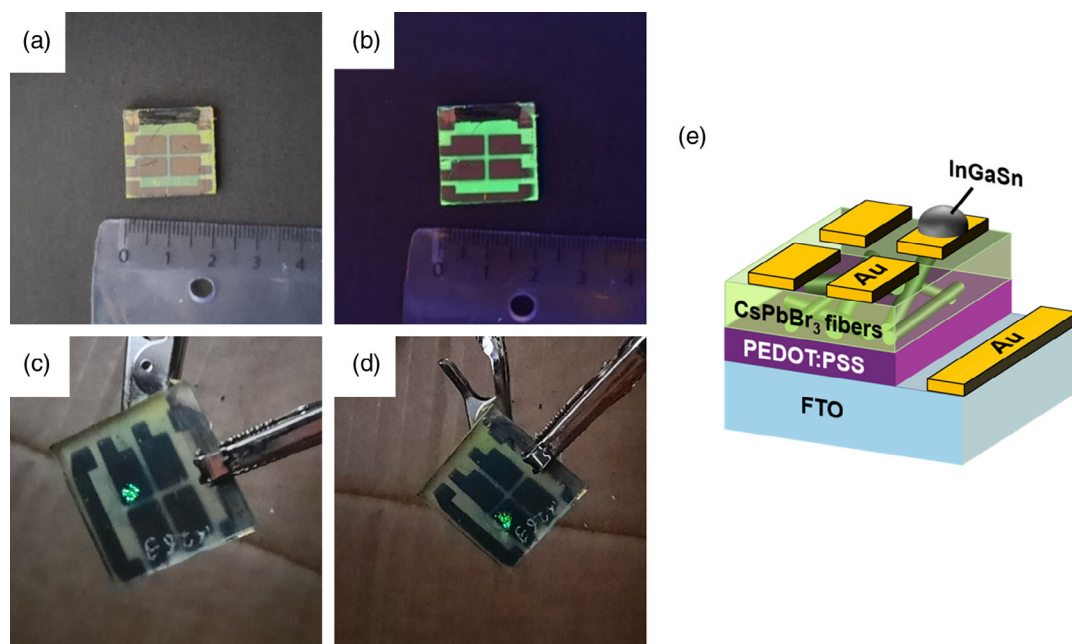


**Figure 7.** a) Photograph of the CsPbBr<sub>3</sub> nanofiber proof-of-concept device b) under UV illumination. c,d) The device with 5 V applied on two different contact areas, and e) scheme of the device.

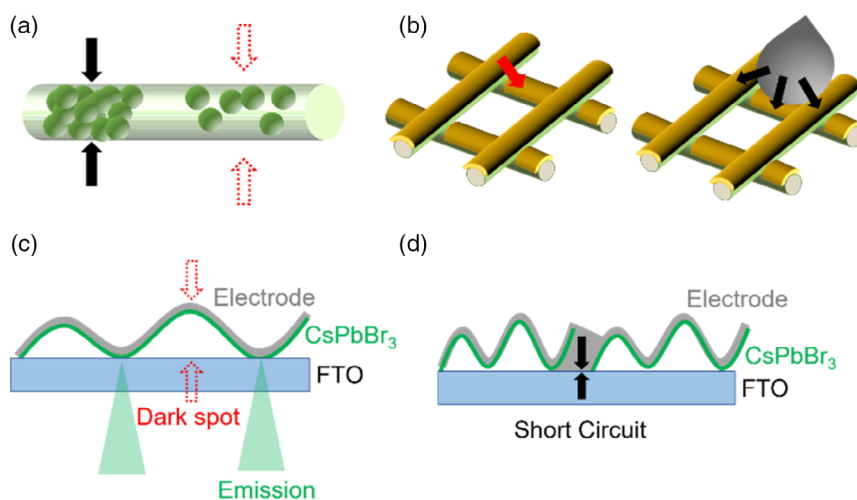


**Figure 8.** Schematics of challenges when contacting the fiber LED. a) If the nanocrystals within the fibers are not interconnected, the insulating polymer matrix hinders charge transport and injection. b) The evaporated gold electrode is not interconnected; thus, the active area as determined by the electrodes is smaller than expected. c) The fiber mat is not flat and thus the charge injection at the elevated areas is not provided. d) The metal electrode (gold or Galinstan) creates a short-circuit path if the fiber mat has holes or scratches.

surface but does not form a closed surface for electrical contacts which could also lead to the necessity of the liquid metal electrode as it can fill the gaps in between the gold-covered fibers (Figure 8b). In addition, we observed that the thickness of the fiber mats is crucial for the functionality in the utilized LED setup, as fiber mats spun for 5 min with the given parameters lead to functional devices while fiber mats spun for 10 min seem to be inoperative. This could be due to worse interconnectivity for thicker fiber mats ( $\approx 10 \mu\text{m}$  compared to  $\approx 4 \mu\text{m}$  for the 5 min spun samples as shown in Figure S7,

Supporting Information) having more insulating polymer and air embedded between the electrodes. The challenge presented in Figure 8a could be overcome by engineering the precursor ink in terms of the ratio between perovskite and polymer to ensure homogenous nanocrystal distribution throughout the fiber. The challenge shown in Figure 8b could be circumvented by evaporation of a thicker gold layer or evaporation while rotating the substrate and tilting in different directions. The solution for the challenges presented in Figure 8c,d could be the fabrication of thicker fiber mats on the substrates and subsequent

pressing to condense the mat and make the layer more even. Initial experiments for device improvement by the suggested methods were unsuccessful and are listed in the Table S2, Supporting Information. Utilization of charge injection layers and the discussed device improvements might enable luminance determination and thus, comparison to current perovskite LED performances. The electroluminescent perovskite fiber device shown here can motivate researchers to investigate and take the concept a step further. As an example, perovskite photovoltaics started with only 3.8% PCE, which was low for state-of-the-art solar cells, but they quickly developed to over 20% in less than 10 years. Perovskite fiber LEDs are in their infancy, but it is interesting to see the versatility of application even with alternative morphologies.

### 3. Conclusions

In this work, EL of electrospun CsPbBr<sub>3</sub> nanofibers was shown for the first time. Furthermore, the perovskite/polymer composite fibers could be prepared under ambient conditions in a one-step spinning process from a solvent mixture of water, ethanol, and the ionic liquid methylammonium propionate. The stability of the water-based precursor ink was tracked and confirmed over 1 month and the fibers were proven to be stable up to at least 5 months under ambient conditions. Compared to their thin-film counterparts, the fabrication of fibers through electrospinning can easily be upscaled while the optoelectronic properties are retained as demonstrated here. The resulting perovskite/polymer composite fibers with diameters of  $\approx 120$  nm consisted of  $\approx 12$  nm perovskite crystallites embedded in a PVP matrix. A proof-of-concept electroluminescent device was built with the prepared perovskite fibers as the emitting layer. These results might push forward functional woven fabrics and flexible optoelectronic devices based on solution-processable perovskite-type materials.

### 4. Experimental Section

**Materials:** All materials were used as received. CsBr (99.9%) and PbBr<sub>2</sub> (99.9%) were purchased from TCI Chemicals. The PEDOT:PSS dispersion type Clevios F CPP105D M was obtained from Heraeus. PVP ( $M_w = 1.300.000$ ) was purchased from Alfa Aesar. Indium–gallium–tin eutectic (“Galinstan”) was obtained from Strategic Elements. MAP was synthesized using a known procedure.<sup>[20]</sup>

**Methods:** For the spin-coating procedures, a SPS Europe Polos Spin 150i infinite spin-coater was used. UV/ozone treatment was done using an ELG 100S UV chamber from Dinies. Evaporation of gold was performed with a Quorum Technologies Q150T S sputter coater. Scanning electron micrographs were acquired with a FEI Strata DualBeam 235 and a Sigma 300 VP by Zeiss equipped with a Xplore 30 by Oxford Instruments for EDX measurements. X-ray diffractometry was done at room temperature on a STOE-Stadi MP with Mo K $\alpha$  source. Evaluation of the micrographs was done manually with ImageJ with the number of counts  $N$  stated in the respective size histograms. UV/vis extinction spectra were recorded in a Lambda 950 UV/vis spectrometer from PerkinElmer. The PL measurements were carried out in an in-house developed sample scanning micro-PL setup. For the excitation of the sample, light from a supercontinuum laser (NKT SuperK Extreme, for the data shown in Figure 5 and S9, Supporting Information) or a mode-locked titanium-sapphire laser (Coherent Chameleon Ultra II, for the data shown in Figure S10, Supporting Information) was used. For the data shown in Figure 5 and

S9, Supporting Information, a bandpass filter with a center wavelength of 433 and 24 nm width was used to select the spectrum of the excitation light. For the data shown in Figure S10, Supporting Information, a band-pass filter with a center wavelength of 405 and 10 nm width was used to select the spectrum of the excitation light. Sample illumination and the emitted light collection were carried out through the same microscope objective (numerical aperture 0.8; MPlanFl, Olympus). Light separation was achieved by a beam splitter and long-pass filters. Spectra were acquired using a grating spectrometer with a deep-cooled charge-coupled device camera (Princeton Instruments). All spectrally integrated signals were recorded with a single-photon-counting module, connected to a fast time tagger (Swabian Instruments) for time-resolved measurements. PLQY measurements were done in an Edinburgh Instruments FLS 980 fluorescence spectrometer using an integrating sphere. The samples were excited with a 450 W ozone-free xenon arc lamp. The detector R928P PMT was electrically cooled to  $-20$  °C. TG measurement was performed using TG/DSC1 (Mettler Toledo GmbH, Germany) apparatus in air with a ramp of  $10$  °C  $\text{min}^{-1}$ . High-resolution transmission electron microscopy was conducted on a JEOL JEM-2200FS at 200 keV. The light stability was examined under 1 sun illumination (1.5 AM, 100 W) with a Solar Simulator Series LS0500 by LOT. Hot pressing was conducted with a T338-AZ by RICOO. All preparations and measurements were conducted at room temperature and in ambient atmosphere unless stated otherwise.

**Procedures:** 183.5 mg PbBr<sub>2</sub> (5 mmol, 1.0 Eq.) and 127.7 mg CsBr (6 mmol, 1.2 Eq.) were mixed with 200 mg PVP ( $M_w = 1.300.000$ ) in a mixture of 1.2 mL H<sub>2</sub>O and 1.0 mL MAP. 40  $\mu\text{L}$  of formic acid were added and the mixture was heated to 60 °C until a clear solution was obtained. For the H<sub>2</sub>O/EtOH mixture, 0.6 mL H<sub>2</sub>O and 0.6 mL EtOH were used instead of 1.2 mL H<sub>2</sub>O. For the PEDOT:PSS containing solution, 1.0 mL Clevios F CPP105D M dispersion was added to the H<sub>2</sub>O/EtOH-based solution after the full dissolution of CsBr, PbBr<sub>2</sub> and PVP. The resulting mixture was stirred for at least 1 h after the addition of the PEDOT:PSS dispersion.

**Fabrication of Light Emitting Device:** Fluorine-doped tin oxide/glass (FTO) from Sigma Aldrich was cut into 2 cm  $\times$  2 cm pieces and cleaned with Hellmanex III detergent, water, and ethanol and placing them in an ultrasonic bath in each solution for 15 min. The substrates were dried with pressurized air and treated in a UV/ozone chamber for 10 min before deposition of PEDOT:PSS. 200  $\mu\text{L}$  Clevios F CPP105D M was spin coated at 2400 rpm for 20 s on the FTO substrate and annealed at 130 °C for 20 min. All fibers were prepared in an ambient atmosphere using a FuG high-voltage DC power supply, a LA-100 syringe pump from Landgraf Laborsysteme, and needles with an inner diameter of 0.514 mm. The distance between the needle and collector was kept at 8 cm and the voltage at 17 kV. The FTO/PEDOT:PSS substrates were placed on a hot plate set to 170 °C and wrapped in aluminum foil and electrospinning was conducted as described before with a duration of 5 min in case of the proof-of-concept light-emitting device. Afterward, 100 nm gold was thermally evaporated on the fibers with a metal mask to determine the deposition area. The final device structure was glass/FTO/PEDOT:PSS/CsPbBr<sub>3</sub> + PVP + PEDOT:PSS composite fibers/Au/Galinstan.

### Supporting Information

Supporting Information is available from the Wiley Online Library or from the author.

### Acknowledgements

The authors gratefully acknowledge the funding and infrastructure provided by the University of Cologne (Excellence Program QM2 “Quantum Matter and Materials”) as well as the framework of the priority program “Perovskite Semiconductors: From Fundamental Properties to Devices” (SPP 2196) of the Deutsche Forschungsgemeinschaft (DFG). This work was carried out in the framework of the Joint Lab GEN\_FAB and was supported by the HySPRINT Innovation Lab at

Helmholtz-Zentrum Berlin. The authors thank Amadi Kingsley Chijioke for thermogravimetric measurements and Nurgül Tosun for support with the transmission electron microscopy sample preparation.

Open Access funding enabled and organized by Projekt DEAL.

## Conflict of Interest

The authors declare no conflict of interest.

## Author Contributions

The manuscript was written through the contributions of all authors. All authors have given approval for the final version of the manuscript.

## Data Availability Statement

The data that support the findings of this study are available from the corresponding author upon reasonable request.

## Keywords

CsPbBr<sub>3</sub>, electrospinning, light-emitting diodes, nanofibers, perovskite

Received: November 15, 2022

Revised: January 17, 2023

Published online: February 16, 2023

- [1] Z. K. Tan, R. S. Moghaddam, M. L. Lai, P. Docampo, R. Higler, F. Deschler, M. Price, A. Sadhanala, L. M. Pazos, D. Credgington, F. Hanusch, T. Bein, H. J. Snaith, R. H. Friend, *Nat. Nanotechnol.* **2014**, *9*, 687.
- [2] M. Kulbak, S. Gupta, N. Kedem, I. Levine, T. Bendikov, G. Hodes, D. Cahen, *J. Phys. Chem. Lett.* **2016**, *7*, 167.
- [3] W. Zheng, Q. Wan, Q. Zhang, M. Liu, C. Zhang, B. Wang, L. Kong, L. Li, *Nanoscale* **2020**, *12*, 8711.
- [4] L. Protesescu, S. Yakunin, M. I. Bodnarchuk, F. Krieg, R. Caputo, C. H. Hendon, R. X. Yang, A. Walsh, M. V. Kovalenko, *Nano Lett.* **2015**, *15*, 3692.
- [5] J. Li, X. Shan, S. G. R. Bade, T. Geske, Q. Jiang, X. Yang, Z. Yu, *J. Phys. Chem. Lett.* **2016**, *7*, 4059.
- [6] Y. Zu, J. Dai, L. Li, F. Yuan, X. Chen, Z. Feng, K. Li, X. Song, F. Yun, Y. Yu, B. Jiao, H. Dong, X. Hou, M. Ju, Z. Wu, *J. Mater. Chem. A* **2019**, *7*, 26116.
- [7] C. Bi, J. Hu, Z. Yao, Y. Lu, D. Binks, M. Sui, J. Tian, *Adv. Funct. Mater.* **2020**, *30*, 2005990.
- [8] L.-M. Chao, T.-Y. Tai, Y.-Y. Chen, P.-Y. Lin, Y.-S. Fu, *Materials* **2015**, *8*, 5467.
- [9] G. Li, Z. Jiang, W. Wang, Z. Chu, Y. Zhang, C. Wang, *Nanomaterials* **2019**, *9*, 50.
- [10] D. Chen, Y. Zhu, *Nanoscale Res. Lett.* **2017**, *12*, 114.
- [11] C. Bohr, M. Pfeiffer, S. Öz, F. von Toperczer, A. Lepcha, T. Fischer, M. Schütz, K. Lindfors, S. Mathur, *ACS Appl. Mater. Interfaces* **2019**, *11*, 25163.
- [12] V. Jamali, F. Niroui, L. W. Taylor, O. S. Dewey, B. A. Koscher, M. Pasquali, A. P. Alivisatos, *Nano Lett.* **2020**, *20*, 3178.
- [13] Q. Shan, C. Wei, Y. Jiang, J. Song, Y. Zou, L. Xu, T. Fang, T. Wang, Y. Dong, J. Liu, B. Han, F. Zhang, J. Chen, Y. Wang, H. Zeng, *Light Sci. Appl.* **2020**, *9*, 163.
- [14] D.-H. Jiang, Y.-H. Tsai, L. Veeramuthu, F.-C. Liang, L.-C. Chen, C. C. Lin, T. Satoh, S.-H. Tung, C.-C. Kuo, *APL Mater.* **2019**, *7*, 111105.
- [15] E. Ercan, P.-C. Tsai, J.-Y. Chen, J.-Y. Lam, L.-C. Hsu, C.-C. Chueh, W.-C. Chen, *ACS Appl. Mater. Interfaces* **2019**, *11*, 23605.
- [16] H. Zhang, D. Fu, Z. Du, H. Fu, G. Shao, W. Yang, J. Zheng, *Ceram. Int.* **2020**, *46*, 18352.
- [17] T. Chen, M. Huang, Z. Ye, J. Hua, S. Lin, L. Wei, L. Xiao, *Nano Res.* **2021**, *14*, 1397.
- [18] Q. Zhang, X. Deng, C. Tan, Y. Zhou, X. Chen, X. Bai, J. Li, B. Tang, S. Li, H. Lin, *J. Chem. Phys.* **2020**, *153*, 24703.
- [19] P. Kumar, N. Ganesh, K. S. Narayan, *ACS Appl. Mater. Interfaces* **2019**, *11*, 24468.
- [20] S. Öz, J. Burschka, E. Jung, R. Bhattacharjee, T. Fischer, A. Mettenböcker, H. Wang, S. Mathur, *Nano Energy* **2018**, *51*, 632.
- [21] N. Yantara, S. Bhaumik, F. Yan, D. Sabba, H. A. Dewi, N. Mathews, P. P. Boix, H. V. Demir, S. Mhaisalkar, *J. Phys. Chem. Lett.* **2015**, *6*, 4360.
- [22] H. Cho, S. H. Jeong, M. H. Park, Y. H. Kim, C. Wolf, C. L. Lee, J. H. Heo, A. Sadhanala, N. S. Myoung, S. Yoo, S. H. Im, R. H. Friend, T. W. Lee, *Science* **2015**, *350*, 1222.
- [23] Y. K. Du, P. Yang, Z. G. Mou, N. P. Hua, L. Jiang, *J. Appl. Polym. Sci.* **2006**, *99*, 23.
- [24] L. Song, X. Guo, Y. Hu, Y. Lv, J. Lin, Z. Liu, Y. Fan, X. Liu, *J. Phys. Chem. Lett.* **2017**, *8*, 4148.
- [25] G. Li, Z.-K. Tan, D. Di, M. L. Lai, L. Jiang, J. H.-W. Lim, R. H. Friend, N. C. Greenham, *Nano Lett.* **2015**, *15*, 2640.
- [26] D. Di, K. P. Musselman, G. Li, A. Sadhanala, Y. Ievskaya, Q. Song, Z.-K. Tan, M. L. Lai, J. L. MacManus-Driscoll, N. C. Greenham, R. H. Friend, *J. Phys. Chem. Lett.* **2015**, *6*, 446.
- [27] J. Li, S. G. R. Bade, X. Shan, Z. Yu, *Adv. Mater.* **2015**, *27*, 5196.
- [28] B. Zhang, L. Goldoni, C. Lambruschini, L. Moni, M. Imran, A. Pianetti, V. Pinchetti, S. Brovelli, L. De Trizio, L. Manna, *Nano Lett.* **2020**, *20*, 8847.
- [29] D. N. Dirin, I. Cherniukh, S. Yakunin, Y. Shynkarenko, M. V. Kovalenko, *Chem. Mater.* **2016**, *28*, 8470.
- [30] C. C. Stoumpos, C. D. Malliakas, J. A. Peters, Z. Liu, M. Sebastian, J. Im, T. C. Chasapis, A. C. Wibowo, D. Y. Chung, A. J. Freeman, B. W. Wessels, M. G. Kanatzidis, *Cryst. Growth Des.* **2013**, *13*, 2722.
- [31] A. D. Wright, G. Volonakis, J. Borchert, C. L. Davies, F. Giustino, M. B. Johnston, L. M. Herz, *Nat. Mater.* **2020**, *19*, 1201.
- [32] Y. Dong, T. Qiao, D. Kim, D. Parobek, D. Rossi, D. H. Son, *Nano Lett.* **2018**, *18*, 3716.
- [33] C. C. Lin, D.-H. Jiang, C.-C. Kuo, C.-J. Cho, Y.-H. Tsai, T. Satoh, C. Su, *ACS Appl. Mater. Interfaces* **2018**, *10*, 2210.